HIGH-EFFICIENCY SOLAR CELLS BASED ON INVERSION LAYER EMITTERS

I. Martín[1], R. Lövblom [2], R. Alcubilla[1]

[1] Departament d'Enginyeria Electrònica, Universitat Politècnica de Catalunya
C/ Jordi Girona 1-3, Mòdul C4, 08034 Barcelona, Spain. Pho.: +34 93 405 41 93
Fax: +34 93 401 67 56, e-mail: isidro@eel.upc.edu

[2] Department of Information Technology and Electrical Engineering (D-ITET), ETH Zurich
Gloriastrasse 35, CH-8092 Zürich, Switzerland, Pho.: +41 44 632 08 34
Fax: +41 44 632 14 92, e-mail: lrickard@ifh.ee.ethz.ch

ABSTRACT: In crystalline silicon (c-Si) solar cells based on p-type substrates, inversion layer emitters have been proposed as an alternative to high-temperature phosphorus diffusion. Dielectric film deposition at low temperature (≤ 400 ºC) is widely used for c-Si surface passivation and in this case emitters are induced by the positive fixed charge, Q_f, at the c-Si/dielectric interface. In this work, we use 2-D simulations to explore solar cell structures with inversion layer emitters placed between local n+-emitters. The local diffusions could be defined by laser processing, resulting in potentially low-temperature processed structures. From simulation results, the low conductivity of inversion layer emitters obligates to short contact spacing and, hence, dense front grids and high shadow losses. However, placing the emitter at the back reduces these penalties, increasing the efficiency about 1% absolute. Furthermore, taking advantage of the fully metallized back surface, inversion layer emitters can be assisted by the workfunction difference between the c-Si substrate and the metal (typically aluminum) over the dielectric. As a result, the necessity of a high positive Q_f value is relaxed.

Keywords: c-Si solar cells, simulation, inversion layer emitters, surface passivation

1. INTRODUCTION

Since the demonstration of the photovoltaic effect, a big effort has been dedicated to increase the conversion efficiency of solar cells based on crystalline silicon (c-Si). The development of surface passivation techniques led to the sophisticated PERL (Passivated Emitter Rear Locally diffused) concept that still holds the record efficiency for non-concentrated sunlight c-Si devices with an outstanding 24.7% [1].

From an industrial point of view, a crucial issue is how to adapt the PERL concept to a low-cost, low-temperature and industrially compatible process. Several technological milestones have paved the way to explore this possibility: low temperature passivating dielectrics, devices based on inversion layers and laser processing. Firstly, the introduction of dielectric films deposited by different techniques at 400ºC or less for c-Si surface passivation avoids the high temperature oxidation step. Among all the studied materials - e.g. amorphous silicon carbide [2], amorphous silicon [3], and more recently, aluminum dioxide [4]- the case of silicon nitride (SiN_x) is particularly successful due to the combination of excellent optical and passivating properties, and nowadays, it is widely applied to industrial c-Si solar cells.

Secondly, to avoid the high temperature step for the creation of n+ emitters, an inversion layer electrostatically induced at the surface of a p-type substrate was proposed. A first approach was the creation of the inversion layer by a low-workfunction semitransparent metal fully covering the front surface [5]. A few years later, the Metal Insulator Semiconductor – Inversion Layer (MIS-IL) solar cell concept was proposed, where the inversion layer is induced by charges within the overlying dielectric film [6-8]. At the early 80's, the SiN_x was firstly applied to MIS-IL solar cells for the creation of the inversion layer because of its high positive interface charge density [9]. The most refined MIS-IL solar cells incorporate Cesium ions at the SiN_x/c-Si interface to increase the fixed charge density. Additionally, the contacts are based on MIS structures with aluminum and a very thin SiO_2, through which the carriers are able to tunnel, resulting in a full low-temperature fabrication process [10].

Finally, laser processing has arisen as a straightforward way for cost savings in both local contact and local emitter formation. Although this idea was applied in photovoltaic devices already in the 80's [11], laser processing of c-Si solar cells has in recent years attracted the interest of the scientific community. A strong research activity is being devoted to the development of contact formation through dielectric films [12], dielectric ablation [13,14], shunted region isolation [15], silicon drilling for Metal/Emitter Wrapped Through solar cells [16], and, of course, p-n junction formation. A first approach for junction fabrication is the emitter formation along the entire cell area by scanning it with a focused laser beam and using a spin-on dopant as a phosphorus source [17,18]. On the other hand, the formation of any desired distribution of the doping profile along the cell surface is extremely simplified when laser processing is used leading to selective emitters. Local diffusions have been proposed [19,20] and even more complicated structures can be defined by guiding the laser radiation into a chemical liquid jet [21].

Within the framework presented above, we propose the creation of local n+ emitters by means of laser processing of passivating dielectrics that contain phosphorus atoms. The idea is that the PECVD film act as a passivation film and a dopant source by the addition of phosphine (PH_3) in the precursor gases. Particularly, in another contribution to this conference [22], our group demonstrates the viability of such structures using phosphorus-doped silicon carbide films.

In this work, we address the design of finished solar cell structures that combine inversion layer emitters and local n+ diffusions through 2-D simulations. Firstly, we revisited the analysis of MIS-IL solar cells reported by Kulhmann et al. [23] illustrating the main drawback of these cells: the necessity of a dense front grid and, hence, too high shadowing losses. In the second part of this

paper, we propose a new structure where the emitter is at the back of the cell. Additionally, we explore the creation of the inversion layer emitter based on the difference in the workfunction of the c-Si and the metal that now fully covers the surface. This structure can relax the necessity of a very high positive Q_f at the dielectric interface.

2. SOLAR CELL MODELLING

The 2D solar cell simulations are carried out with the Synopsys TCAD tool suite. Since the main purpose of this study is the comparison of different solar cell design concepts, it is vital that the simulations of all devices are carried out within one well-defined framework of physical and geometrical models. Among all them, the substrate doping density and the fixed charge at the dielectric interface are critical parameters because they control the inversion layer formation. We chose 1.1×10^{16} cm^{-3} and 10^{12} cm^{-2} respectively that are typical values in the state of the art of c-Si solar cells and guarantee a strong inversion at the surface. The rest of simulation parameters used in this work are compiled in the Appendix.

Accurate computation of surface generation-recombination rates, inversion layer carrier concentrations, etc., places stringent requirements on the refinement of the simulation grid, and dense vertical grid spacing in the order of 1 nm is mandatory in the surface region. Due to the lateral periodicity of the solar cell geometry, it is usually sufficient to simulate a region with a width corresponding to half of the front contact spacing, which relaxes the computation requirements. Such simplifications have successfully been employed in 2D and 3D-simulations of similar cell structures [24,25].

Figure 1 depicts the simulation domains studied in this work labeled as: Front side Inversion Layer Emitter (FILE), Front side Low Doped Emitter (FLDE), and Back side Inversion Layer Emitter (BILE). The FLDE and FILE structures are equivalent, replacing the low doped emitter under the passivating film by an inversion layer induced by the fixed charge located at the c-Si/dielectric interface. These structures are used to investigate the effect of the front contact spacing, d_f, ranging from 100 µm to 2.5 mm. Finally, the BILE cell has a constant d_f of 800 µm and a variable rear contact spacing, d_r, shorter or equal to d_f.

By transferring a 3-D device to a 2-D simulation domain, certain geometrical features are simplified to such an extent that they strongly deviate from their actual three-dimensional structure. In our case, the most prominent examples are the highly doped regions under the contacts. Circular regions are expected in the final device, but for the 2-D structure the geometrical information in the depth direction is lost. Then, instead of points, the extrapolation of the highly doped regions into the depth direction leads to lines. Nevertheless, these distortions do not invalidate any of the conclusions of this work.

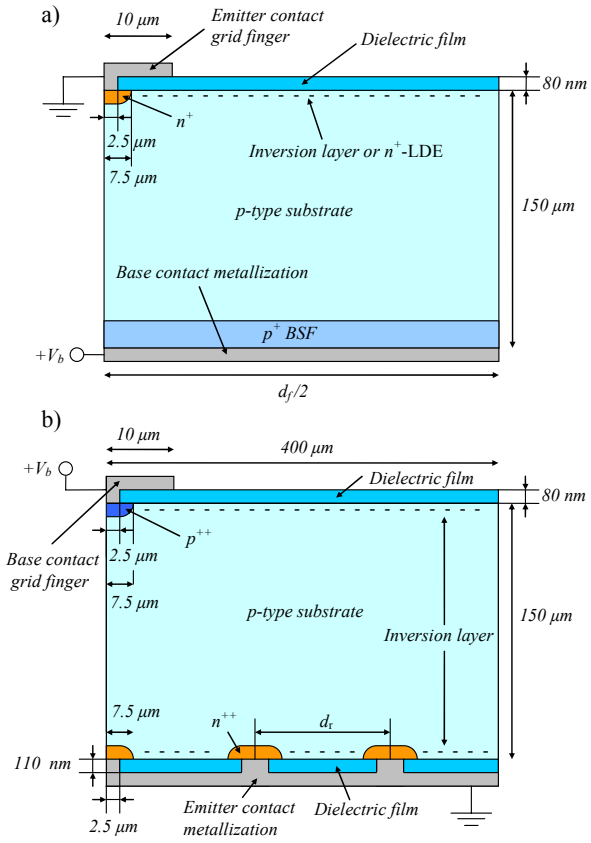

Figure 1. Schematic representations of the simulation domains of the (a) FILE and FLDE, and (b) BILE cells.

3. COMPARISON OF FILE AND FLDE CONCEPTS

Firstly, we compare two structures with the emitter at the front side where the inversion layer emitter (FILE) is replaced by a conventional low doped emitter (FLDE). The difficulties of using inversion layer emitters were already explored by Kulhmann et al. for simulations of MIS-IL solar cells [23]. The conclusions of that work are also valid for our purposes since the only difference is the configuration of the contacts (MIS structure instead of conventional n+ diffusion). However, the simulations of FILE and FLDE structures presented hereby help us to illustrate the problems involving inversion layer emitters. In addition, since the structures are simulated under the same physical and geometrical framework, we can use them as a reference for the new structure proposed in the next section of this paper.

From the work of Kulhmann et al., we can conclude that a critical parameter of these cells is the front contact spacing. In Figure 3, V_{oc}, J_{sc}, FF and η of the FILE cell (empty symbols) varying front contact spacing, d_f, are shown. For comparison, the corresponding structure with a low doped emitter under the passivating film (FLDE cell, filled symbols) is also simulated and the results are plotted in the same graphs.

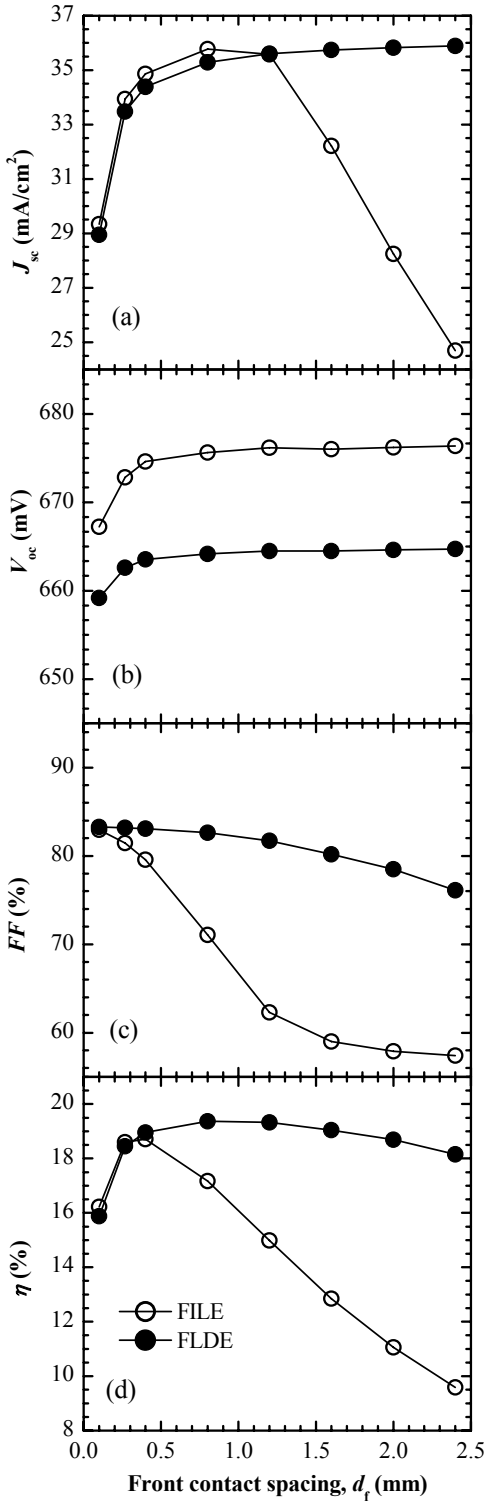

Figure 2. FILE cell (empty symbols) and FLDE cell (filled symbols); (a) short-circuit current density (J_{sc}), (b) open-circuit voltage (V_{oc}), (c) conversion efficiency (η) and (d) fill factor (FF) versus front contact spacing, d_f.

Focusing on the conversion efficiency, one can see that the FLDE cell maintains its efficiency throughout the explored d_f range, whereas the efficiency of the FILE cell rapidly decreases when d_f is beyond 0.5 mm. This trend is linked to the FF. When the front contacts are separated, the induced emitter introduces a high series resistance drastically reducing the FF. At d_f = 1.2 mm, a change in the slope is observed. At this point, the ohmic losses in the emitter become higher than those associated with the current path through the substrate and the emitter does no longer function as a collecting junction. Now, the photogenerated carriers travel laterally through the bulk to the contacts, and the sheet resistance of the substrate is limiting *FF*.

Additionally, a strong decrease in the short-circuit current density can be observed at this point. Without an extended n-p junction, the central region in between contacts is not biased and is kept under open-circuit conditions. Then, the photogenerated carriers must travel longer distances to reach the collecting junction dramatically increasing their recombination.

In agreement with Kuhlmann et al. [23], it can be concluded that the main drawback of the FILE structure is the necessity of a short front contact spacing (lower than approximately 0.5 mm) and, thus, dense front metal grids. In order to reduce the penalty for the high shadowing losses, we propose to turn around the structure, relocating the emitter to the rear of the cell. This is presented in the following section.

4. BACK SIDE INVERSION LAYER EMITTER (BILE) CELL

4.1 Advantages compared to FILE cell.

The structure of the BILE cell is shown in figure 1.b): the n+ emitter is at the rear of the cell with the same configuration as in the FILE structure, whereas the front surface corresponds to a local BSF structure. This structure is potentially fabricated in a full low-temperature process if laser processing is applied to the highly-doped region formation. Now, the rear contact spacing becomes critical as the inversion layer emitter is located at the back. In figure 3, we show the V_{oc}, J_{sc}, FF and η of the BILE cell varying rear contact spacing, d_r, with aluminum (triangles) completely covering the rear surface.

The first result is that FF has a similar trend as in the FILE cell leading to $d_r < 0.5$ mm for FF higher than 80%. The limitation in contact spacing is the same as in the FILE cell, but in this case it does not impact on the shadowing factor. In fact, J_{sc} is constant and higher than the values obtained for FILE cells with $d_f < 0.5$ mm. This is a direct result of the larger separation between the grid fingers (0.8 mm) reducing the shadowing factor. However, the increase in J_{sc} is less than this geometrical factor predicts. Due to the high blue-component of AM1.5 spectrum, most of the carriers are generated at the first microns close to the front surface. The collecting junction is now at the rear and, thus, their recombination probability increases resulting in additional losses not present at the FILE cell. Moreover, excellent surface passivation at the front surface becomes mandatory. On the other hand, V_{oc} increases with d_r due to better surface passivation. Combining all these results, about 1% absolute in conversion efficiency is gained compared to the FILE cell.

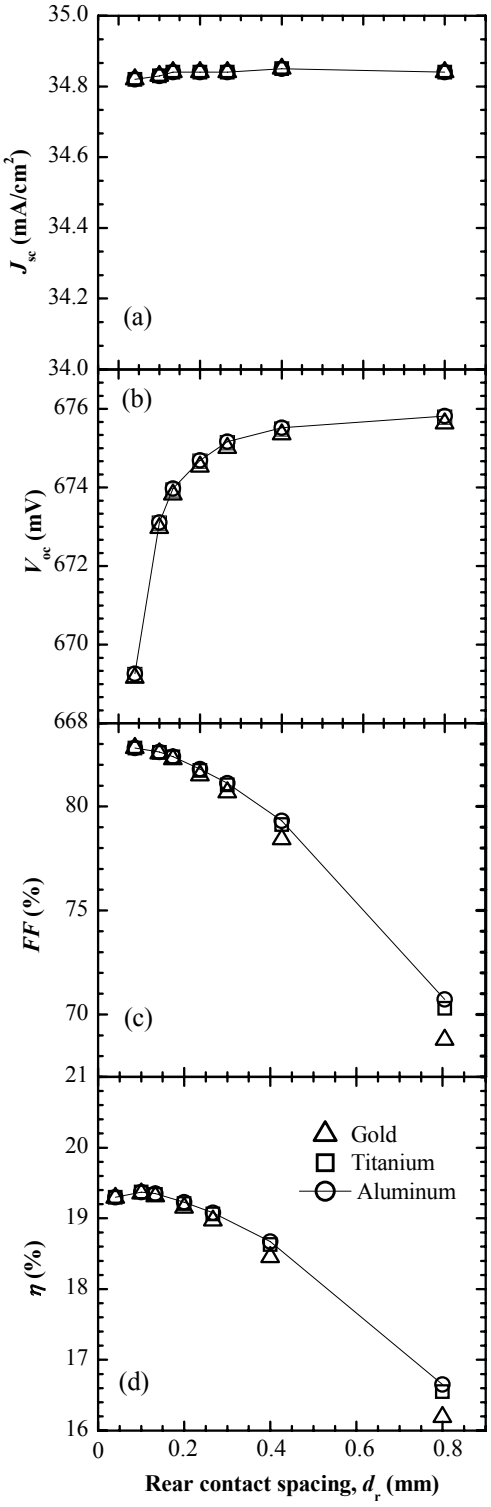

Figure 3. BILE cell with aluminum (triangles), titanium (circles) or gold (squares) fully covering the back surface; (a) short-circuit current density (J_{sc}), (b) open-circuit voltage (V_{oc}), (c) conversion efficiency (η) and (d) fill factor (FF) versus rear contact spacing, d_r.

Since the rear surface is partially configured as a MIS system, we have also investigated the effect of the metal workfunction (Φ_m) for the metal that fully covers it. Apart from aluminum (Φ_m = 4.2 eV), we also used titanium (Φ_m = 4.4 eV) and gold (Φ_m = 5.0 eV) in order to explore a wide Φ_m range. From the simulation results, the most significant effect is a small reduction in the FF with the largest simulated rear contact spacing (d_r = 800 μm): from 71.7% with aluminum to 68.8% with gold. The relatively high Q_f value of 10^{12} cm^{-2} defined at the SiN_x/c-Si interface is dominant and metals with high workfunction (similar to the one of the p-type substrate) can slightly weaken the inversion layer emitter by reducing the induced electric field.

4.2 Inversion layer emitters based on workfunction difference.

Up to now, the inversion layer emitter is based on a high positive Q_f value. However, this parameter is prone to be affected by multiple physical aspects, e.g. dielectric composition, interface cleanness, thermal stability, etc., and, hence, it is difficult to tune. In addition, for relatively highly doped substrates, there may be difficulties in achieving the minimum value for a correct operation of the induced emitter. So, a new question arises: can we obtain an induced emitter less linked to Q_f? This is possible in BILE structures due to the fact that the induced emitter is located in regions with a MIS configuration. Consequently, the difference in workfunction between the p-type c-Si substrate and the metal can help to induce the emitter. In order to explore the limits of this idea, we simulate an extreme case: a BILE structure with no Q_f at the back surface and aluminum as the back contact metal resulting in a workfunction difference of 0.87 eV. The dielectric capacitance at the rear surface, C_d, is taken as a parameter, since this magnitude directly affects the capability of the metal to induce the emitter. It is defined as $C_d = \varepsilon_r\varepsilon_0 / t_d$, where ε_r is the relative dielectric constant, ε_0 the dielectric constant under vacuum and t_d is the dielectric thickness. Simulation results are shown in Figure 4 for C_d ranging from 51 μF/cm^2 to 6637.5 μF/cm2. Notice that an equivalent SiN_x thickness with ε_r = 7.5 is also indicated in the secondary x-axis of the first plot as a reference. For example, the explored C_d range corresponds to a SiN_x films between 1 nm and 135 nm.

As it can be seen, conversion efficiency decreases with C_d up to 110 nF/cm^2 (60 nm-thick SiN_x film) and increases again beyond this point. As the dielectric thickness increases and, consequently, C_d decreases from its maximum value, a weaker inversion layer is induced raising the recombination rate at the back surface. The increased recombination at the rear mainly has impact on the dark saturation current of the diode and, hence, on V_{oc}, while only a small variation is expected in J_{sc} since very few carriers are generated close to the rear surface. At $C_d \approx$ 110 nF/cm2, the electron and hole densities at the surface are equal under open-circuit conditions, resulting in a minimum in V_{oc}. Furthermore, beyond this point the inversion layer vanishes and, hence, J_{sc} also decreases as it did in the case of the FILE cell (see Figure 2). Finally, FF follows a trend that is similar to the one observed in the V_{oc}, indicating that the FF variations are related to the dependence of back surface recombination on injection level leading to non-ideal dark I-V curves. Additionally, the small back contact spacing (0.1 mm) avoids a strong increase in series resistance when the inversion layer disappears. From these results, we can conclude that good efficiencies can be obtained for inversion layer emitters based on the difference between workfunctions. Nevertheless, relatively thin dielectrics must be used. Such thin dielectrics fully covered with

metal must be of excellent quality in order to prevent shunts. It must be mentioned that the thickness reduction is limited by tunneling effect in the MIS structure, not included in these simulations.

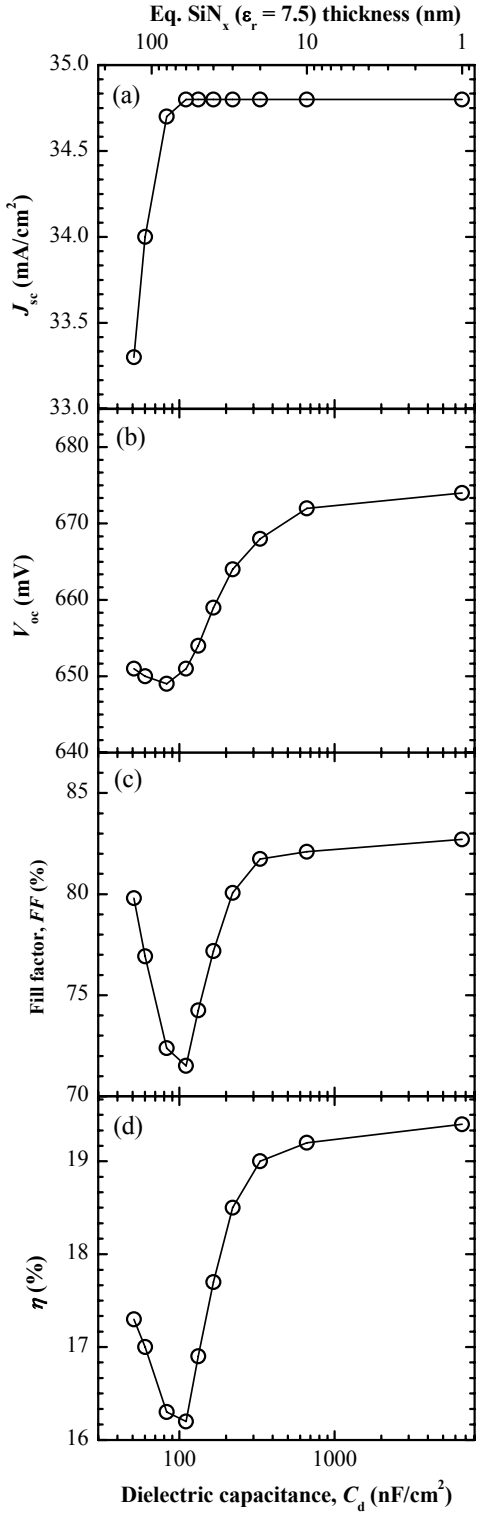

Figure 5. BILE cell where the emitter is induced by the difference in workfunction between Aluminum and p-type c-Si substrate, $\Delta\Phi$ = 0.87 eV; (a) short-circuit current density (J_{sc}), (b) open-circuit voltage (V_{oc}), (c) conversion efficiency (η) and (d) fill factor (FF) versus dielectric thickness at the rear surface, t_d.

5. CONCLUSIONS

Based on 2-D simulations, we analyzed the advantages and drawbacks of different solar cells that can be potentially processed at low temperature (< 400ºC) based on deposited surface passivating films, inversion layer emitters and laser processing. The high ohmic losses of the inversion layer obligate to a very short distance between front contacts, typically < 0.5 mm, and very dense front grids. The relocation of the inversion layer the back of the cell results in higher potential efficiencies due to the reduction in shadowing losses. Furthermore, in these structures the inversion layer can be formed based on the difference in workfunction between the p-type substrate and the aluminum that fully covers the surface. As a consequence, the necessity of a high positive Q_f value is relaxed.

ACKNOWLEDGMENTS

This work has been supported by the Spanish Government through the projects TEC-2008-02520/TEC and PSE-MICROSIL08 (PS-120000-2006-6).

References

[1] J. Zhao, A. Wang, M.A. Green, Proceedings of 21st IEEE Photovoltaic Specialists Conference, 333 (1990).
[2] I. Martín, M. Vetter, A. Orpella, J. Puigdollers, A. Cuevas, R. Alcubilla, Appl. Phys. Lett. 79, 2199 (2001).
[3] S. Dauwe, J. Schmidt, R. Hezel, Proceedings of 29th IEEE Photovoltaic Specialists Conference, 1246 (2002).
[4] B. Hoex, S.B.S. Heil, E. Langereis,M.C.M. van de Sanden, V.M.M. Kessels, Appl. Phys. Lett. 89, 042112 (2006).
[5] W.A. Anderson, A.E. Delahoy, R.A. Milano, J. Appl. Phys. 45, 3913 (1974).
[6] G.C. Salter, R.E. Thomas, Solid State Electronics, 20, 95 (1977).
[7] P. van Halen, R.P. Mertens, R.J. van Overstraeten, R.E. Thomas, J. van Meerbergen. IEEE Trans. Electron Devices 25, 507 (1978).
[8] R.B. Godfrey, M.A. Green, Appl. Phys. Lett. 34, 790 (1979).
[9] R. Hezel, R. Schoerner, J. Appl. Phys. 52, 3076 (1981).
[10] R. Hezel, Progr. Photovolt. Res. Appl. 5, 109 (1997).
[11] E. Fogarassy, R. Stuck, J.J. Grob, P. Siffert, J. Appl. Phys. 52, 1076 (1981).
[12] E. Schneiderlöchner, R. Preu, R. Lüdemann, S.W. Glunz, Progr. Photovolt. Res. Appl. 10, 29 (2002).
[13] S.A.G.D. Correia, J. Lossen, M. Wald, K. Neckermann, M. Bärh, Proceedings of 22nd European Photovoltaic Solar Energy Conference, 1061 (2007).
[14] A. Grohe, A. Knorz, M. Aleman, C. Harmel, S.W. Glunz, R. Preu, G.P. Willeke, Proceedings of 21st European Photovoltaic Solar Energy Conference, 750 (2006).
[15] Y. Augarten, M.D. Abbott, T. Trupke, R. Bardos, H.P. Hartmann, R. Gupta, J. Bauer, O. Breitenstein, Proceedings of 22nd European Photovoltaic Solar Energy Conference, 1220 (2007).
[16] S. Hermann, P. Engelhart, A. Merkle, T. Neubert, T. Brendemühl, R. Meyer, N. Harder, R. Brendel Proceedings 22nd European Photovoltaic Solar Energy Conference, 970 (2007).

[17] A. Esturo-Breton, M. Ametowobla, C. Carlsson, J. Köhler, J. Werner, Proceedings of 21st European Photovoltaic Solar Energy Conference, 1247 (2006).
[18] K. Horiuchi, Y. Nishihara, A. Ogane, Y. Takahashi, A. Kitiyanan, Y. Uraoka, T. Fuyuki, Proceedings of 22nd European Photovoltaic Solar Energy Conference, 1423 (2007).
[19] S.W. Glunz, A. Grohe, M. Hermle, E. Schneiderlöchner, J. Dicker, R. Preu, H. Mäckel, D. Macdonald, A. Cuevas, Proceedings of 3rd World Conference Photovoltaic Energy Conversion, 1332 (2003).
[20] B.S. Tjahjono, J.H. Guo, Z. Hameiri, L. Mai, A. Sugianto, S. Wang, S.R. Wenham, Proceedings of 22nd European Photovoltaic Solar Energy Conference, 966 (2007).
[21] S. Hopman, A. Fell, K. Mayer, M. Aleman, M. Mesec, R. Müller, D. Kray, G.P. Willeke, Proceedings of 22nd European Photovoltaic Solar Energy Conference, 1257 (2007).
[22] A. Orpella, I. Martín, S. Blanque, C. Voz, I. Sánchez, M. Colina, C. Molpeceres, R. Alcubilla, *"Optimization of laser processes in n^+ emitter formation for c-Si solar cells",* presented in this conference.
[23] B. Kuhlmann, A.G. Aberle, R. Hezel, G. Heiser, IEEE Trans. on Electron Devices 47, 2167 (2000).
[24] G. Heiser, P.P. Altermatt, J. Litsios, Proceedings of 6th IEEE Conference on Simulation of Semiconductor Devices and Processes, 348 (1995).
[25] H.S. Bennet, C.L. Wilson, J. Appl. Phys. 55, 3582 (1984).
[26] G. Masetti, M. Severi, S. Solmi, IEEE Trans. on Electron Devices 30, 764 (1983).
[27] C. Canali, G. Majni, R. Minder, G. Ottaviani, IEEE Trans. on Electron Devices 22, 1045 (1975).
[28] C. Lombardi, S. Manzini, A. Saporito, M. Vanzi, IEEE Trans.s on Computer-Aided Design of Integrated Circuits and Systems 7, 1164 (1988).
[29] S.W. Glunz, Advances in OptoElectronics 2007, 97370 (2007).

APPENDIX

Table I. Summary of the most relevant parameters used in the simulations

Carrier statistics	Fermi-Dirac, complete ionization of impurities
Badgap narrowing	Bennet-Wilson model [25] modified to yield $n_{i,eff} = 9.99987\times10^{9}$ cm^{-3} for $N_A=1.1\times10^{16}$ cm^{-3}
Carrier mobility	Doping-dependent (Masetti model [26]), high-field saturation (Canali model [27]) and surface mobility degradation (Lombardi mode [28])
Recombination	
Shockley-Read-Hall (bulk)	Defect level at midgap, doping-dependent $\tau_{n0} = \tau_{p0} = \tau_0$ $$\tau_0 = \frac{2.4\times10^{-4}}{1+\frac{N_{dop}}{10^{16}}} \text{ (s)}$$ (where N_{dop} is the doping concentration; this expression yields 0.11 ms for $N_A = 1.1\times10^{16}$ cm^{-3})
Auger	Injection-dependent Auger coefficients
Radiative	C = 1.1×10^{-14} cm^{3}s^{-1}
Doping parameters	
Bulk acceptor density, N_A	1.1×10^{16} cm^{-3}
Back surface field (BSF)	Gaussian distribution of boron atoms, surf. conc. of 5×10^{18} cm^{-3}, junction depth of 5 μm for $N_A =1\times10^{16}$ cm^{-3}
n^{++} and p^{++} regions	Gaussian distribution of phosphorus or boron atoms, surf. concentration 10^{20} cm^{-3}, junction depth 1 μm for $N_A =1\times10^{16}$ cm^{-3}
Low doped emitter (LDE)	Gaussian distribution of phosphorus atoms, surf. concentration 5×10^{18} cm^{-3}, junction depth 0.6 μm for $N_A =1\times10^{16}$ cm^{-3}
Interface parameters	
Fixed charge density, Q_f	10^{12} cm^{-2}
Shockley-Read-Hall (surf.)	Defect level at midgap, doping-dependent $S_{n0} = S_{p0} = S_0$ $$S_0 = 50\left(1+\frac{N_{dop}}{10^{16}}\right) \text{ (cm/s)}$$ (this expression yields S_0 = 105 cm/s for $N_A = 1.1\times10^{16}$ cm^{-3})
Optical parameters	
Incident light spectrum	AM 1.5g with an irradiance of 0.1 W/cm^2
Front reflectivity	Front reflections determined by Transfer Matrix Method (TMM). Dielectric film with n = 1.9.
Back reflectivity	Wavelength independent reflectivity defined as $$R_{back} = R_m\left(\frac{5}{d_r}\right) + R_{MIS}\left(1-\frac{5}{d_r}\right)$$ where R_m denotes the reflectivity of the metallized regions (83% [29]), R_{MIS} denotes the reflectivity of the MIS-regions (assumed to be 100%) and d_r is the back contact spacing in μm. For BSF configuration a fixed R_{back} = 65% is used [29].